Electronic structure of the benzene dimer cation

Piotr A. Pieniazek, Anna I. Krylov, and Stephen E. Bradforth
Department of Chemistry, University of Southern California, Los Angeles, California 90089-0482

(Received 20 March 2007; accepted 22 May 2007; published online 31 July 2007)

The benzene and benzene dimer cations are studied using the equation-of-motion coupled-cluster model with single and double substitutions for ionized systems. The ten lowest electronic states of the dimer at t-shaped, sandwich, and displaced sandwich configurations are described and cataloged based on the character of the constituent fragment molecular orbitals. The character of the states, bonding patterns, and important features of the electronic spectrum are explained using qualitative dimer molecular orbital linear combination of fragment molecular orbital framework. Relaxed ground state geometries are obtained for all isomers. Calculations reveal that the lowest energy structure of the cation has a displaced sandwich structure and a binding energy of 20 kcal/mol, while the t-shaped isomer is 6 kcal/mol higher. The calculated electronic spectra agree well with experimental gas phase action spectra and femtosecond transient absorption in liquid benzene. Both sandwich and t-shaped structures feature intense charge resonance bands, whose location is very sensitive to the interfragment distance. Change in the electronic state ordering was observed between σ and π_u states, which correlate to the $\tilde{B}$ and $\tilde{C}$ bands of the monomer, suggesting a reassignment of the local excitation peaks in the gas phase experimental spectrum. © *2007 American Institute of Physics*. [DOI: 10.1063/1.2749506]

I. INTRODUCTION

The benzene dimer has attracted considerable attention as a model system for studying π-π interactions, which influence secondary structures of biological molecules, such as proteins, RNA, and DNA,[1–5] host-guest complexes,[6–8] and molecular recognition.[9] Their understanding is vital for controlling molecular organization in solid and liquid states.[10] Photoinduced processes in these complex systems involve electronic excitation and subsequent charge transfer and localization in which the extended aromatic π system is the key player.[11–15] In addition, oxidative damage induced either chemically or by radiation in DNA leads to aromatic radical cations. Solvents used in radioactive element separation are susceptible to radiation induced ionization, which in the case of neat aromatic liquids leads to the formation of aromatic cations and dimer cations such as $(C_6H_6)_2^+$ and $(C_5H_5N)_2^+$.[16–18] The benzene dimer cation is thus a prototype for studying ionization-induced processes in noncovalent aromatic complexes, neat liquids, and aggregates.

From an electronic structure point of view, ionization of a van der Waals dimer changes formal interfragment bond order from zero to half-integer and, therefore, switches interaction from noncovalent to covalent. This has a profound effect on the strength of interaction and the structure of the dimer: for example, the helium dimer is bound by only 11.009 K (0.000 95 eV) and the corresponding equilibrium distance is about 5.6 bohr,[19] while He_2^+ has D_e=2.5 eV and r_e=2.04–2.06 bohr.[20] In the case of nonspherical fragments, the relative orientation of the monomers may also change upon ionization. Electronic excitation, especially to diffuse Rydberg orbitals, may have a similar effect, and rare gas or aromatic excimers are well known examples.[21–25] In the benzene dimer, additional complexity arises due to high symmetry of the monomer, which results in degenerate states of $C_6H_6^+$ that undergo Jahn-Teller (JT) distortions.[26–28] Both intramolecular and intermolecular degrees of freedom may be involved.

The shapes of the cation potential energy surfaces (PESs) are determined by the character of molecular orbitals (MOs) hosting a hole. For example, ionization from a bonding (from the dimer point of view) MO yields a repulsive PES, whereas ionization from an antibonding orbital results in a bound potential. In both cases, the magnitude of the effect depends on the overlap between fragment MOs. Thus, ionization from the more compact inner orbitals will have a less profound effect on interfragment bonding, and the resulting states will be just like the perturbed localized states of the monomers. Consequently, the electronic spectrum of the dimer cation will feature two types of transitions: those similar to the monomers, as well as transitions unique to the dimer, that is, transitions between the states derived from ionization of strongly overlapping outer orbitals. Since the overlap depends strongly on the interfragment distance and relative orientation, dynamics of the dimer cation can be monitored through the changes in its electronic spectrum, just as in excimer studies.[29,30]

Experimentally, the dimer cation has been characterized in the gas phase by Nishi and co-workers.[31–34] Photodissociation action spectra revealed absorption at 2.82, 2.14, 1.35, and 1.07 eV. The former two bands have been assigned as local excitations (LEs), whereas the latter two have been assigned as charge resonance (CR) bands, that is, transitions unique to the dimer. In solid glasses, γ irradiated liquid benzene exhibits bands at 2.64 and 1.36 eV,[35] the latter band being assigned to benzene dimer cation based on its similarity to that observed in irradiated paracyclophanes.[36] In the

liquid phase, photoionization of neat benzene leads to an intense transient absorption band assigned to a dimer cation core at 1.35 eV.[16] This is consistent with the adiabatic ionization energy (IE) of the neutral dimer being 8.65 eV,[37,38] significantly lower than 9.24 eV of the monomer.[28] Ground state binding energy (BE) in the gas phase has been measured to be in the range 15–20 kcal/mol.[37–43]

Several computational studies have investigated the ground state structures of the dimer cation.[41,43–47] Milosevich *et al.*[44] suggested a displaced sandwich structure based on Hartree-Fock calculations. Møller-Plesset calculations of Hiraoka *et al.*[41] put forward the t-shaped structure as the lowest isomer. Density functional calculation predicts the ground state to have a sandwich structure.[43,47] The most exhaustive study to date is due to Miyoshi *et al.*,[45,46] who characterized both ground and excited states of the dimer cation. In the earlier work,[45] they employed the complete active space self-consistent field (CASSCF) and multireference configuration interaction with singles and doubles (MR-CISD) methods to investigate the electronic structure of sandwich, displaced sandwich, and t-shaped isomers. The lowest energy structure at the CASSCF level was the t-shaped isomer. Inclusion of dynamical correlation at the MR-CISD and MR-CISD with Davidson correction levels changed the relative energies in favor of the displaced sandwich isomer. Electronically excited states derived by ionization of a single π electron have also been calculated at the first-order configuration interaction level.

Unfortunately, transition dipoles and oscillator strengths have not been reported. The later study explored a larger set of isomers and accounted for intramolecular relaxation.[46] The best estimates of the cation binding energies (calculated at the multireference coupled pair approximation level) were 12.3 and 5.4 kcal/mol for the displaced sandwich and t-shaped isomers, respectively. The authors have also explored the nature of the four lowest excited charge resonance states at tilted and displaced sandwich configurations. Contrary to the experimental results,[31] they predicted the more intense CR band to occur at a lower energy than the less intense one. The excited state pattern in the tilted structure did not match the experimental spectrum.

The goal of this work is to characterize low-lying electronic states of $(C_6H_6)_2^+$ and to outline how the bonding and electronic spectra change upon relevant geometrical distortions. We start by briefly reviewing the electronic structure of the neutral dimer and $C_6H_6^+$ in Sec. II. We then develop a general MO framework for describing the electronic states in ionized noncovalent dimers, in the spirit of exciton theory.[23,48] Further in Sec. III B, we apply our MO framework to develop classification of the electronic states of the benzene dimer cation that combines symmetry and bonding properties. After this qualitative analysis, we present vertical ionization energies and the electronic spectra of the cation at equilibrium geometries of the neutral dimer. To describe the evolution of the electronic spectra with geometry changes from neutral to cation and to estimate the relaxed structures of $(C_6H_6)_2^+$, we present scans along several relaxation coordinates. Finally, we briefly discuss connections to the experimental studies and outline future work. The EPAPS document contains coordinates of the optimized monomer and relaxed dimer structures, as well as energies of PES scans.[49]

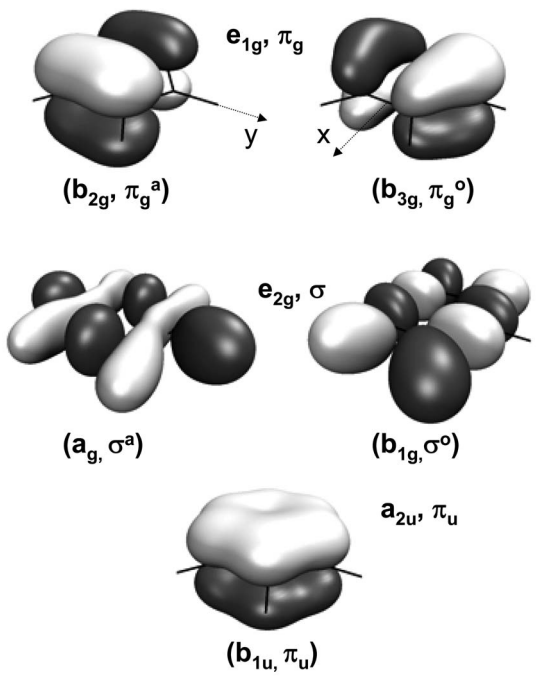

FIG. 1. The five highest occupied orbitals of neutral benzene. Both D_{6h} and D_{2h} symmetry labels are given.

II. PREREQUISITES: BONDING IN THE NEUTRAL BENZENE DIMER AND BENZENE CATION

The lowest energy structure of $(C_6H_6)_2$ has been the subject of controversy, as the three major isomers are very close in energy and their structures are floppy.[50–55] The most accurate estimate of D_0 (close to *ab initio* limit) by Sinnokrot and Sherrill[55,56] gives the following values for the sandwich, displaced sandwich, and t-shaped structures: 1.81, 2.78, and 2.74 kcal/mol, respectively. Podeszwa *et al.*[57] obtained a six-dimensional PES of $(C_6H_6)_2$ using symmetry-adapted perturbation theory of intermolecular interactions based on density functional theory description of monomers. Using this PES, they found that a tilted t-shaped isomer is the lowest energy one, with a BE of 2.77 kcal/mol. The BEs of the sandwich and displaced sandwich isomers were found to be 1.87 and 2.74 kcal/mol, respectively. Zero-point energy correction changed the BE of the tilted t-shaped isomer to 2.46 kcal/mol and that of the displaced sandwich to 2.42 kcal/mol. Experimental results are consistent with the t-shaped isomer as the lowest energy structure.[53]

In our calculations of vertical ionization energies, we employed equilibrium structures of the three isomers from Sinnokrot and Sherrill's work. Ionization changes interaction from noncovalent to covalent, which results in larger D_e and shorter r_e. Moreover, as follows from the simple MO overlap considerations, ionization also significantly affects the relative energies of the three isomers. We conducted several PES scans along important relaxation coordinates, which are presented in Sec. V B, along with our estimates of equilibrium structures and D_e for the dimer cation.

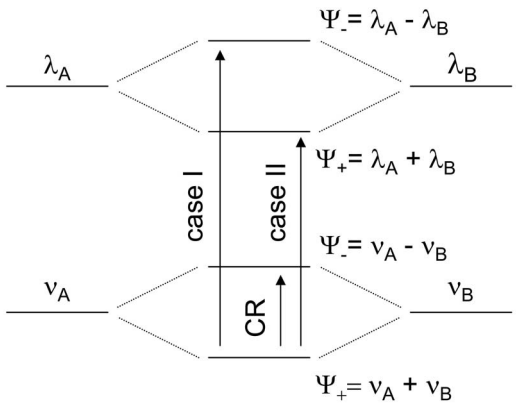

FIG. 2. FMOs and DMOs of an *AB* dimer. See Sec. III A for details.

Unlike the dimer cation, the ionized states of C_6H_6 have been extensively characterized both experimentally[58–61] and theoretically.[62–65] The highest occupied MOs of the neutral benzene are presented in Fig. 1. The corresponding vertical IEs are 9.45, 11.7, and 12.3 eV, from the e_{1g}, e_{2g}, and a_{2u} orbitals, respectively.[59] At the D_{6h} geometry, the cation ground state is doubly degenerate and $C_6H_6^+$ undergoes Jahn-Teller distortions to two lower-symmetry D_{2h} structures, which are best described as an acute and an obtuse structure. The minimum energy structure has been the subject of intensive research, and it has been found that the acute structure is the energy minimum, whereas the obtuse structure is, in fact, a transition state. The experimental energy difference between the two is merely 8 cm^{-1}.[26] The geometries of the cation states used in our calculations have been optimized using equation-of-motion ionization potential (EOM-IP)-CCSD/6-311G*.[49] The optimized acute cation structure is 1417 cm^{-1} below the D_{6h} equilibrium structure of the neutral, whereas the obtuse structure is 1404 cm^{-1} lower. Despite a relatively low level of theory, the calculated difference of 13 cm^{-1} is in excellent agreement with the experimental value. Section V A presents our calculations of IEs and transition properties between different cation states at select geometries.

III. ELECTRONIC STRUCTURE OF IONIZED NONCOVALENT DIMERS

A. Dimer molecular orbital linear combination of fragment molecular orbital (DMO-LCFMO) framework

In this section, we develop a qualitative molecular orbital description of the electronic structure of the dimer, in the spirit of exciton theory.[23,48] In analogy to molecular orbitals linear combination of atomic orbital description of diatomics, we describe the dimer MOs (DMOs) as linear combinations of the fragment MOs. This framework results in a convenient dimer state nomenclature and will be applied to explain the trends in the electronic state ordering, oscillator strengths, and structural relaxation. We also discuss the electronic structure of ionized dimers in terms of charge-localized pseudodiabatic states, as is often done in the context of charge transfer reactions.[66–68]

We begin our DMO-LCFMO treatment by introducing MOs localized on fragments A and B: $\nu_{A,B}$ and $\lambda_{A,B}$. For equivalent fragments, the DMOs are just symmetric and antisymmetric linear combinations of the FMOs, as shown in Fig. 2 and in the equations below:

$$\psi(\nu) = \psi_+(\nu) = \frac{1}{\sqrt{2(1+s_{\nu\nu})}}(\nu_A + \nu_B), \tag{1}$$

$$\psi^*(\nu) = \psi_-(\nu) = \frac{1}{\sqrt{2(1-s_{\nu\nu})}}(\nu_A - \nu_B), \tag{2}$$

where the subscript denotes to which monomer the FMO belongs, and ψ_+ and ψ_- refer to the bonding and antibonding (with respect to interfragment interaction) DMOs. $s_{\nu\nu}$ is the overlap between the monomer MOs:

$$s_{\nu\nu} = \langle \nu_A | \nu_B \rangle. \tag{3}$$

Likewise, $\psi_\pm(\lambda)$ will refer to the bonding and antibonding DMO pair derived from the monomer orbitals λ_A and λ_B. Similar notation is used in molecular electronic structure, recall, for example, $\sigma(2p_z)$ in O_2 or $\pi(p_y)$ and $\pi^*(p_y)$ in ethylene. When this naming scheme is applied to the benzene dimer MOs (Sec. III B), $\sigma^*(\pi_u)$ refers to the antisymmetric combination of the monomer π_u orbitals, and so on.

Following the H_2^+ textbook exercise, the energy splitting between one-electron states $\psi_\pm(\nu)$ can be trivially worked out and shown to be proportional to the overlap integral $\langle \nu_A | \nu_B \rangle$.[69] The stabilization energy (with respect to isolated monomers) is simply half of this splitting.

Each pair of doubly occupied MOs of the monomers gives rise to two dimer orbitals and a formal zero bond order. Ionization results in the three-electron-in-two-orbital wave function, which can be mapped to the one-electron-in-two-orbital one. For example, the bond order of the $(\psi_+(\nu))^2(\psi_-(\nu))^1$ configuration is the same as that of $(\psi_+(\nu))^1(\psi_-(\nu))^0$. Furthermore, the $\psi_+ \rightarrow \psi_-$ transition in the former is equivalent to $\psi_+ \rightarrow \psi_-$ in the latter, in terms of the symmetry and the resulting changes in bond order. However, the motion of the hole in the three-electron-in-two-orbital picture is opposite to the motion of the electron in one-electron-in-two orbitals, and the $(\psi_+(\nu))^2(\psi_-(\nu))^1 \rightarrow (\psi_+(\nu))^1(\psi_-(\nu))^2$ excitation is isomorphic with $(\psi_+(\nu))^1(\psi_-(\nu))^0 \rightarrow (\psi_+(\nu))^0(\psi_-(\nu))^1$. Note that the symmetry of the initial and final states is reversed in the one-electron-in-two-orbital [initial state has a symmetry of $\psi_+(\nu)$] system relative to the three-electron-in-two-orbital one [initial state has a symmetry of $\psi_-(\nu)$]. The transition symmetry, defined as the direct product of the symmetries of the two states, remains unchanged. Due to the Hermitian nature of the transition dipole moment operator, the transition dipole moments are identical in both cases.

With the above considerations, electronic states of an ionized van der Waals dimer can be mapped to those of H_2^+, and we will frequently refer to this example to demonstrate general conclusions of the model. In the case of H_2^+, the ν and λ orbitals from Fig. 2 could be the $1s$ and $2p$ orbitals of the H atom.

We will consider three different types of transitions between the dimer levels. First, there are two types of transi-

tions between ν and λ manifolds, cases I and II from Fig. 2. These are called local excitation bands, as they correlate with the electronic transitions of isolated fragments. In H_2^+, these correspond to $\sigma(1s)\rightarrow\sigma^*(2p_z)$, $\sigma(1s)\rightarrow\pi^*(2p_x)$, $\sigma(1s)\rightarrow\sigma(2p_z)$, etc., transitions that correlate with $1s\rightarrow 2p$ excitations in H. The third type is specific for the dimer/diatomic and involves transitions within the same manifold, i.e., CR bands, as the $\sigma(1s)\rightarrow\sigma^*(1s)$ transition in H_2^+.

Transition dipoles for the case I and II electronic transitions from Fig. 2 are

$$\langle\psi_+(\nu)|\mu|\psi_\pm(\lambda)\rangle = \frac{1}{2\sqrt{(1+s_{\nu\nu})(1\pm s_{\lambda\lambda})}}(\langle\nu_A|\mu|\lambda_A\rangle \pm\langle\nu_B|\mu|\lambda_B\rangle+\langle\nu_B|\mu|\lambda_A\rangle\pm\langle\nu_A|\mu|\lambda_B\rangle). \tag{4}$$

The relationship between the integrals above (i.e., intrafragment AA vs BB and interfragment AB vs BA), as well as the symmetry of orbitals $\psi_\pm$, depends on how the inversion (in the dimer frame) operator $\hat{i}$ acts on ν and λ. Consider first

$$\hat{i}\nu_A=\nu_B \quad \text{and } \hat{i}\lambda_A=\lambda_B$$

or

$$\hat{i}\nu_A=-\nu_B \quad \text{and } \hat{i}\lambda_A=-\lambda_B. \tag{5}$$

In diatomics, the symmetric case is the case when ν and λ are s orbitals, and the corresponding ψ_+ and ψ_- are then *gerade* and *ungerade*, respectively. The antisymmetric case corresponds to $p_{x,y}$ orbitals, and the corresponding bonding and antibonding orbitals are ungerade and gerade. In both cases, $\langle\nu_A|\mu|\lambda_A\rangle=-\langle\nu_B|\mu|\lambda_B\rangle$ and $\langle\nu_A|\mu|\lambda_B\rangle=-\langle\nu_B|\mu|\lambda_A\rangle$. Thus, the transition dipole is zero for $\psi_+(\nu)\rightarrow\psi_+(\lambda)$, as it should be for gerade$\rightarrow$gerade and ungerade$\rightarrow$ungerade transitions. The $\psi_+(\nu)\rightarrow\psi_-(\lambda)$, i.e., case I, transition is symmetry allowed, as $\psi_+(\nu)$ and $\psi_-(\lambda)$ are of different symmetry, and the transition dipole is

$$\langle\psi_+(\nu)|\mu|\psi_-(\lambda)\rangle = \frac{1}{\sqrt{(1+s_{\nu\nu})(1-s_{\lambda\lambda})}}(\langle\nu_A|\mu|\lambda_A\rangle+\langle\nu_B|\mu|\lambda_A\rangle). \tag{6}$$

Similarly, when

$$\hat{i}\nu_A=\nu_B \quad \text{and } \hat{i}\lambda_A=-\lambda_B$$

or

$$\hat{i}\nu_A=-\nu_B \quad \text{and } \hat{i}\lambda_A=\lambda_B, \tag{7}$$

the signs of the integrals from Eq. (4) change and $\langle\psi_+(\nu)|\mu|\psi_-(\lambda)\rangle$ is zero, while

$$\langle\psi_+(\nu)|\mu|\psi_+(\lambda)\rangle = \frac{1}{\sqrt{(1+s_{\nu\nu})(1+s_{\lambda\lambda})}}(\langle\nu_A|\mu|\lambda_A\rangle+\langle\nu_B|\mu|\lambda_A\rangle). \tag{8}$$

Equations (6) and (8) are essentially identical equations describing gerade-ungerade transition. From the bonding perspective, however, the first case is a bonding-antibonding transition, whereas the second is a bonding-bonding excitation.

In H_2^+, if $\nu\equiv 1s$ and $\lambda\equiv 2p_z$, both orbitals transform identically under the inversion, as in Eq. (5), and case I transitions, e.g., $\sigma(1s)\rightarrow\sigma^*(2p_z)$, are allowed, while case II, $\sigma(1s)\rightarrow\sigma(2p_z)$, transitions are forbidden. If, however, $\lambda\equiv 2p_{x,y}$, orbitals transform according to Eq. (8) $\sigma(1s)\rightarrow\pi^*(2p_{x,y})$ and $\sigma(1s)\rightarrow\pi(2p_{x,y})$ excitations are forbidden and allowed, respectively.

Let us now consider how the intensities of case I and case II transitions, which are given by Eqs. (6) and (8), respectively, depend on the interfragment separation. In the united atom limit ($R_{AB}=0$) the transition becomes $\nu_A\rightarrow\lambda_A$, and its transition dipole assumes the monomer value. At large R_{AB}, the interfragment term in Eqs. (6) and (8) vanishes, as the overlap integral decays exponentially with the distance, and the transition dipole is, again, the same as in the monomer. At intermediate distances, both the intrafragment and interfragment terms may contribute. Our results for the dimer indicate that the contribution of the former is much smaller around equilibrium separations.

For the CR transitions, i.e., when $\nu=\lambda$, Eq. (4) assumes the following form:

$$\begin{aligned}\langle\psi_+(\nu)|\mu|\psi_-(\nu)\rangle &= \frac{1}{2\sqrt{(1-s_{\nu\nu}^2)}}(\langle\nu_A|\mu|\nu_A\rangle-\langle\nu_A|\mu|\nu_B\rangle \\ &\quad +\langle\nu_B|\mu|\nu_A\rangle-\langle\nu_B|\mu|\nu_B\rangle) \\ &= \frac{1}{2\sqrt{(1-s_{\nu\nu}^2)}}(\langle\nu_A|\mu|\nu_A\rangle-\langle\nu_B|\mu|\nu_B\rangle).\end{aligned} \tag{9}$$

At large R_{AB}, the difference between the two terms is just the difference between the average positions of monomers A and B, i.e., the interfragment distance R_{AB}, and we arrive to

$$\langle\psi_+(\nu)|\mu|\psi_-(\nu)\rangle \approx \frac{R_{AB}}{2\sqrt{1-s_{\nu\nu}^2}}. \tag{10}$$

Thus, the transition dipole of such transitions increases linearly with the fragment separation. This corresponds to the transitions between complementary bonding-antibonding orbitals,[70] i.e., so-called charge transfer or charge resonance transitions (see Fig. 2). As the oscillator strength depends also on the energy splitting between $\psi_+(\nu)$ and $\psi_-(\nu)$, it will, therefore, go to zero at large R_{AB}. These types of transitions are unique for the dimers, and the charge resonance band in $(C_6H_6)_2^+$ discussed below is of this type.

When the monomers are very different, as in the t-shaped isomer, the DMOs become similar to the localized FMOs and so are the resulting states. Thus, the electronic spectrum of the dimer will be similar to that of the monomers, unless considerable delocalization occurs. DMO-LCFMO can be applied to the case of nonequivalent fragments as well, explaining the consequences of the symmetry reduction (see Appendix).

When the monomers are similar, as in slightly deformed sandwiches or in diatomics composed of atoms with similar

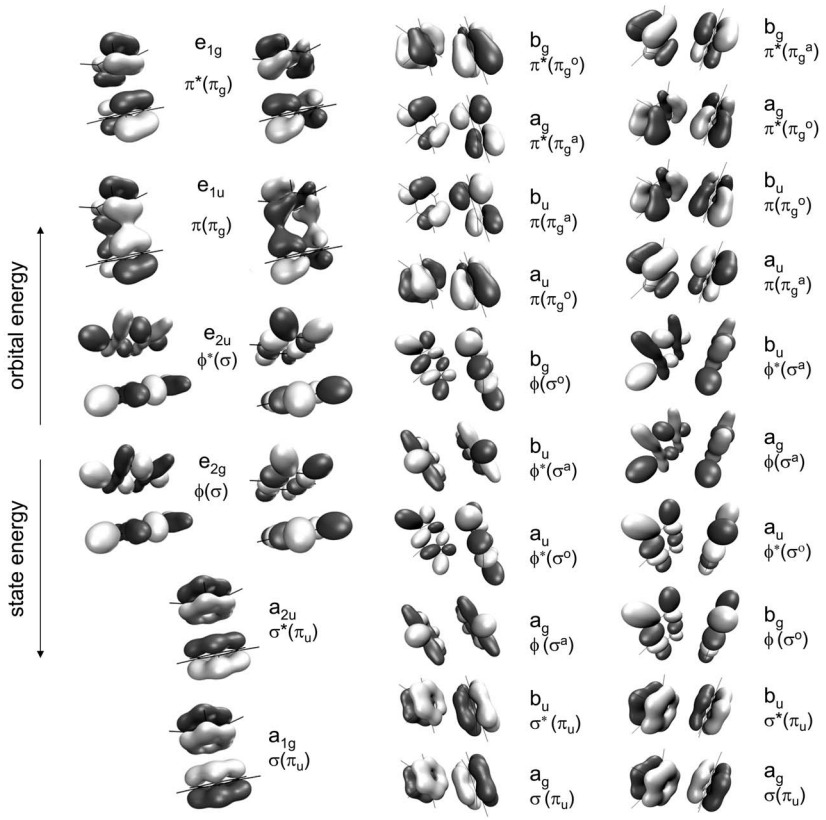

FIG. 3. Highest occupied molecular orbitals of $(C_6H_6)_2$ at (a) D_{6h}, (b) x-, and (c) y-displaced sandwich configurations.

electronegativity, the MOs retain some of their complementary bonding-antibonding character, giving rise to strong CR bands. The intensity of a CR band is proportional to the interfragment separation, decreasing with distance due to the exponential decays of the transition energy. Regardless of how nonequivalent the fragments are, the intensities of the LE bands will be similar to that of the monomers.

Finally, we would like to point out that the dimer states can also be described in terms of pseudodiabatic charge-localized states. The wave functions for the diabatic states can be expressed in the FMO basis as follows:

$$\psi_{A^+B} = (\nu_A)^0(\nu_B)^1,$$
$$\psi_{AB^+} = (\nu_A)^1(\nu_B)^0. \tag{11}$$

In H_2^+, these would correspond to the electron being localized on one of the $1s$ orbitals. When monomers are equivalent the diabatic states are degenerate, and the coupling thus is just half the splitting between the *adiabatic* states. In the case of nonequivalent monomers, the coupling can be inferred using the generalized Mulliken-Hush model.[71]

B. Orbital and state nomenclature for the benzene dimer cation

Below we apply the DMO-LCFMO framework to the low-lying states of the benzene dimer cation. For the sandwich-type isomers, each benzene unit is treated as an atom, and the line connecting the centers of the monomers plays the role of a bond axis. The orbital character is assigned based on the nodal structure in the plane perpendicular to the bond. Orbitals will be named as described above, that is, by specifying their character with respect to the fragments, as well as the type of the constituent FMOs, similar to $\sigma(2s)$ or $\sigma^*(p_z)$ notations in diatomics. As will become obvious, this is not only useful for explaining properties of the states but also allows us to navigate through the ten electronic states of each of the four isomers. The overall symmetry labels, although important, are not very helpful here, as they mask the character of the states, and, most importantly, change upon geometry distortions. For example, although the states of the sandwich and displaced sandwich isomers are very similar, their symmetry labels are different, as the symmetry of the latter is lowered from D_{6h} to C_{2h}.

The ten highest occupied MOs (HOMOs) of the benzene dimer are formed by linear combination of the five highest MOs of each neutral monomer (see Fig. 1). As mentioned in Sec. II, in the monomer the ionization from highest degenerate orbital pair gives rise to two degenerate states that undergo Jahn-Teller distortion to either acute or obtuse angle D_{2h} structures, e.g., ionization from the b_{2g} component leads to an acute angle configuration, whereas ionization from b_{3g} leads to an obtuse angle structure. Thus, we will refer to these orbitals as π_g^a and π_g^o, respectively. The e_{1g} orbitals are of σ character, and the corresponding ion states exhibit similar JT distortions. Thus, these MOs will be denoted as σ^a and σ^o, respectively. Finally, the lowest a_{1u} orbital will be called π_u. The superscript will be dropped when referring to orbitals derived from either one of the two degenerate MOs.

Below we discuss the MOs of the sandwich isomers and the t-shaped dimer. The MOs at all three sandwich structures, which are shown in Fig. 3, are very similar. The highest MOs in the sandwich isomer, the e_{1g} pair, are formed from out-of-

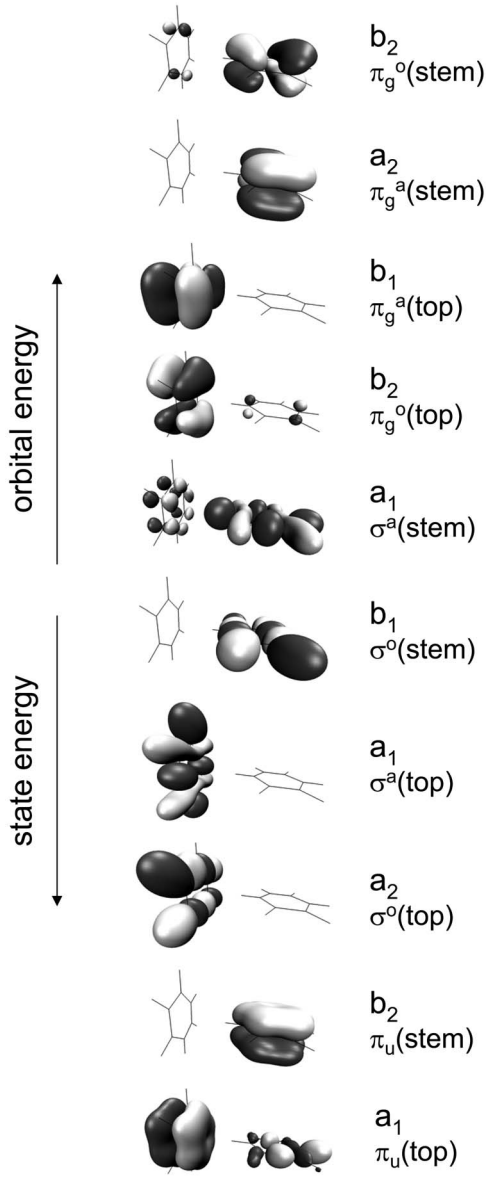

FIG. 4. Highest occupied molecular orbitals of t-shaped $(C_6H_6)_2$.

phase combinations of the π_g^a and π_g^o monomer orbitals. The e_{1u} in-phase combinations are lower in energy. With respect to the dimer, these orbitals are of π character. Thus, the two e_{1g} components are named $\pi^*(\pi_g^a)$ and $\pi^*(\pi_g^o)$, whereas the e_{1u} orbitals are called $\pi(\pi_g^a)$ and $\pi(\pi_g^o)$. When rings slide relative to each other, the degeneracy of both pairs is lifted and their symmetry labels are changed; however, the resulting MOs retain their π-like character. The next two pairs are the e_{2g} and e_{2u} orbitals formed by in-phase and out-of-phase combinations of σ_g^o and σ_g^a. Their nodal structure in the benzene plane is similar to ϕ-type diatomic orbitals. Thus, the out-of-phase combination is referred to as $\phi^*(\sigma^a)$ and $\phi^*(\sigma^o)$, whereas the in-phase combination is called $\phi(\sigma^a)$ and $\phi(\sigma^o)$. Finally, the out-of-phase (a_{2u}) and in-phase a_{1g} combinations of the monomer π_u orbitals are called $\sigma^*(\pi_u)$ and $\sigma(\pi_u)$.

The MOs of the t-shaped isomer are shown in Fig. 4. As the monomers are no longer equivalent, the resulting orbitals are more localized, as in heteronuclear diatomics. We will refer to them by specifying their monomer character and whether they are localized on the stem or the top fragments. For example, the HOMO is called π_g^o(stem), whereas the lowest orbital is called π_u(top). Several orbitals feature discernible delocalization between the top and stem fragments, for example, the π_g^o(stem) and the π_g^o(top) are actually unequal mixtures of π_g^o orbitals of the monomers. Similarly, the σ^a(stem) and π_u(top) are mixtures of the respective fragment orbitals. The delocalization increases at shorter distances. An interesting feature of the electronic level pattern is that the orbitals of the top fragment are lower in energy than the orbitals of the stem molecule. This is further discussed in Sec. V C.

IV. THEORETICAL METHODS AND COMPUTATIONAL DETAILS

Describing open-shell states is a challenging task for *ab initio* methodology, especially in the case of orbital (near) degeneracies. In the case of ionized dimers, even the ground state description is problematic due to symmetry breaking and spin contamination of doublet Hartree-Fock references, and the problems are only exacerbated for the excited states. EOM-IP-CCSD (Refs. 72–75) overcomes these difficulties by describing the problematic open-shell doublet wave functions Ψ (cation) as ionized and excited states of a well-behaved neutral wave function Ψ (neutral):

$$\Psi(\text{cation}) = (\hat{R}_1 + \hat{R}_2)\Psi(\text{neutral}), \tag{12}$$

where Koopmans-type operators R_1 and R_2 generate all possible ionized and ionized and excited configurations out of the closed-shell reference determinant, and Ψ (neutral) is a coupled cluster with single and double substitutions (CCSD) wave function of the neutral.

Our recent benchmark study[76] demonstrated that this approach yields smooth potential energy surfaces and accurate energy splittings, both for symmetric and asymmetric configurations. Thus, the t-shaped and sandwich configurations are described with equal accuracy and their relative stability can be determined. In the case when fragments are distinguishable, the extent of charge localization is also more accurately reproduced using EOM-IP-CCSD rather than doublet reference CCSD (Refs. 77) and equation-of-motion coupled cluster with single and double substitutions for excitation energies [EOM-EE-CCSD (Refs. 78 and 79)].

Below, we first present relevant results for the five lowest electronic states of the benzene cation, and then proceed to the dimer. All calculations were performed at the EOM-IP-CCSD level, using the QCHEM *ab initio* package.[80] The 1*s* core orbitals of carbon were frozen when specified. In addition to calculation of vertical IEs, we also conducted several PES scans along the important interfragment relaxation coordinates.

The equilibrium geometry of C_6H_6 (r_{CC}=1.3915 Å and r_{CH}=1.0800 Å) was taken from Ref. 81. The $^2B_{2g}$ and $^2B_{3g}$ state geometries of $C_6H_6^+$ were optimized by EOM-IP-CCSD/6-311G* with tight convergence criteria. The resulting structures are presented in the EPAPS data.[49] The ionization energies were calculated using EOM-IP-

TABLE I. Vertical ionization energies (eV) of benzene calculated using EOM-IP-CCSD/6-31+G* with frozen core.

	e_{1g}	e_{2g}	a_{2u}
6-31G	8.83	11.65	12.19
6-31+G*	9.12	11.98	12.44
6-31+G* FC	9.10	11.98	12.46
6-311+G*	9.18	12.04	12.52
6-311(2+,2+)G**	9.24	12.12	12.58
Expt.[a]	9.45	11.7	12.3

[a]Reference 59.

CCSD with 6-31G, 6-31+G*, 6-311+G*, and 6-311(2+,2+)G* basis sets. In the frozen core calculation, the six 1*s* orbitals were frozen.

All dimer calculations were performed at the EOM-IP-CCSD/6-31+G* level of theory with core orbitals frozen. The geometries of neutral t-shaped, sandwich, and *x*-displaced sandwich structures were taken from Ref. 55. This set was augmented by a displaced sandwich structure, in which benzene rings are slipped in the *y* direction. The intermolecular coordinates were adapted from the structure displaced in the *x* direction. In the relaxation studies the minimum energy point was located with 0.1 Å precision. For the t-shaped isomer the intermolecular distance was varied from 9.0 to 4.1 Å. Similarly, the interplanar distance of the sandwich isomer was changed from 9.0 to 2.7 Å. In the case of the displaced sandwich isomer, after preliminary checks, detailed scans were performed at 3.0, 3.1, and 3.2 Å interplanar distances. The displacement was varied from 0 to 1.6 Å in the *x* and *y* directions separately. In all calculations, monomer rings were held at their neutral equilibrium geometry. Also, at each geometry the IEs of the ten lowest electronic states were calculated. Finally, ionization energies, transition dipole moments, and oscillator strengths for transitions between electronic states of $(C_6H_6)_2^+$ were computed at both neutral and relaxed dimer cation geometries. Relaxed geometries are included in the EPAPS data.

V. RESULTS

A. Electronic structure of the benzene cation

Table I compares experimental vertical IEs with the values calculated using various basis sets. Overall, IEs increase with the basis set size. With the largest basis set employed, 6-311(2+,2+)G**, the IE to the $^2E_{2g}$ (π_g) state is still underestimated by 0.2 eV, whereas IEs to the $^2E_{1g}$ (σ) and $^2A_{2u}$ (π_u) states are overestimated by 0.4 and 0.3 eV, respectively. Freezing the core electrons has a small effect on the IEs. The basis set dependence of energy differences between the cation states, i.e., the difference of corresponding IEs, is much weaker due to error cancellation, e.g., the calculated changes are less than 0.1 eV for all the basis sets. The energies of the $^2E_{2g} \rightarrow {}^2E_{1g}$ ($\tilde{B}$ band) and $^2E_{2g} \rightarrow {}^2A_{2u}$ ($\tilde{C}$ band) transitions are overestimated by 0.6 and 0.5 eV, respectively.

TABLE III. Estimated binding energies of $(C_6H_6)_2^+$ at various configurations.

Configuration	ΔE (kcal/mol)
Neutral	
t-shaped	10.74
Sandwich	13.94
x-displaced sandwich	14.77
y-displaced sandwich	14.86
Relaxed	
t-shaped	12.40
Sandwich	18.34
x-displaced sandwich	20.14
y-displaced sandwich	20.18

The electronic state ordering of $C_6H_6^+$ along with transition properties at select geometries is summarized in Table II. All the energies are relative to the $^2E_{1g}$ (π_g) state at the neutral geometry. As expected, the $^2B_{2g}$ (π_g^a) state favors the acute geometry due to antibonding character of the orbitals with respect to two parallel carbon-carbon bonds, while $^2B_{3g}$ (π_g^o) state prefers the obtuse geometry due to antibonding character with respect to two opposite apexes. Consequently, its energy increases when the cation is distorted to the acute geometry. The ^2A_g (σ^a) and $^2B_{1g}$ (σ^o) are actually destabilized by either distortion but the variations are much smaller. $^2B_{1g}$ (π_u) is stabilized relative to the neutral geometry for both acute and obtuse angle displacements. Due to these effects, both the $\pi-\pi$ and $\pi-\sigma$ excitations are blueshifted upon JT relaxation, the magnitude being larger in the latter case. At the neutral geometry, the corresponding target states are separated by 0.45 eV, which agrees well with 0.5 eV difference in vertical IEs. At the cation geometries the difference decreases to 0.19/0.34 eV. Only small variation of the transition dipole moment is observed.

In summary, the computational method employed underestimates the IE to the $^2E_{1g}$ state of the benzene monomer by

TABLE II. Energies (eV), transition dipole moments (a.u.), and oscillator strengths for the transitions from the ground state benzene cation at various geometries.

Acute				Neutral				Obtuse			
	E_{ex}	μ	f		E_{ex}	μ	f		E_{ex}	μ	f
B_{2g}/π_g^a	−0.178			E_{1g}/π_g	0.00			B_{3g}/π_g^o	−0.176		
B_{3g}/π_g^o	0.265	⋯	⋯					B_{2g}/π_g^a	0.258	⋯	⋯
A_g/σ^a	2.919	⋯	⋯	E_{2g}/σ	2.881	⋯	⋯	B_{1g}/σ^o	2.910	⋯	⋯
B_{1g}/σ^o	3.072	⋯	⋯					A_g/σ^a	3.075	⋯	⋯
B_{1u}/π_u	3.262	0.923	0.072	A_{2u}/π_u	3.329	0.947	0.0731	B_{1u}/π_u	3.259	0.919	0.0710

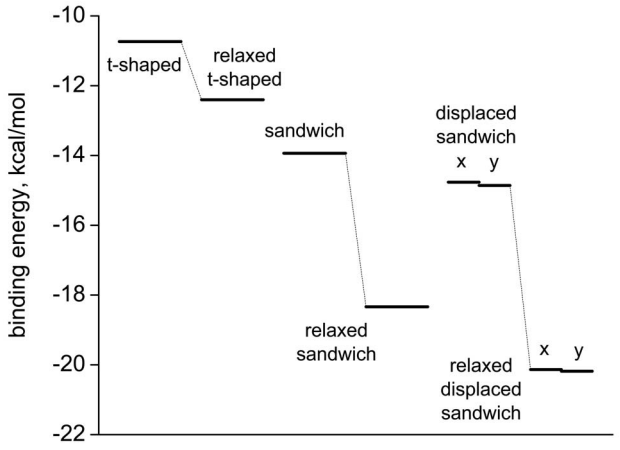

FIG. 5. Estimated binding energies of different $(C_6H_6)_2^+$ isomers.

0.35 eV and overestimates IEs to the $^2E_{2g}$ and $^2A_{2u}$ states by 0.3 and 0.15 eV, respectively. This leads to overestimating the corresponding excitation energy. JT relaxation to nearly degenerate acute and obtuse geometries increases the splitting between the ground and excited states.

B. Potential energy scans, structural relaxation, and binding energies of the dimer cation isomers in the ground electronic state

In this section, we consider PES scans of the dimer cation along several relaxation coordinates. In these calculations we ignored JT distortions and kept the monomers frozen at their neutral geometry.[81] Table III and Fig. 5 summarize estimates of BE at various interfragment configurations, assuming dissociation into the $C_6H_6^+$ and C_6H_6 species, both at the neutral benzene equilibrium geometry. First, we calculated BEs at the geometries of the three $(C_6H_6)_2^+$ isomers from Ref. 55. Then we have augmented this set by a displaced sandwich structure in which the ring is moved in the *y* direction. For the t-shaped and sandwich isomers, the PES along the interfragment distance was scanned. In the displaced isomers, the slipping coordinate was also scanned. In all these cases, minima were located with 0.1 Å precision.

As expected from the MO considerations (see Introduction) ionization increases the BE of the dimer and results in tighter structures. It also changes the relative energy ordering of the isomers. The t-shaped structure, a candidate for the lowest energy isomer of the neutral benzene dimer, happens to be the highest in the cation. The binding energy at this configuration increases from 2.6 kcal/mol in the neutral to 10.7 kcal/mol in the cation. Allowing the intermolecular distance to relax from 5.0 to 4.6 Å further increases this value to 12.4 kcal/mol. However, the relaxed t-shaped structure is still higher in energy than the sandwich, in which BE is 13.9 kcal/mol at the neutral separation of 3.9 Å. In the cation, the interfragment distance relaxes to 3.3 Å, and the binding energy increases to 18.3 kcal/mol. Both in the neutral and the cation benzene dimer, the symmetric sandwich structures appear to be transition states between the displaced structures, possibly due to the JT effect. In the neutral, the rings move by 1.6 Å in the *x* direction with a separation of

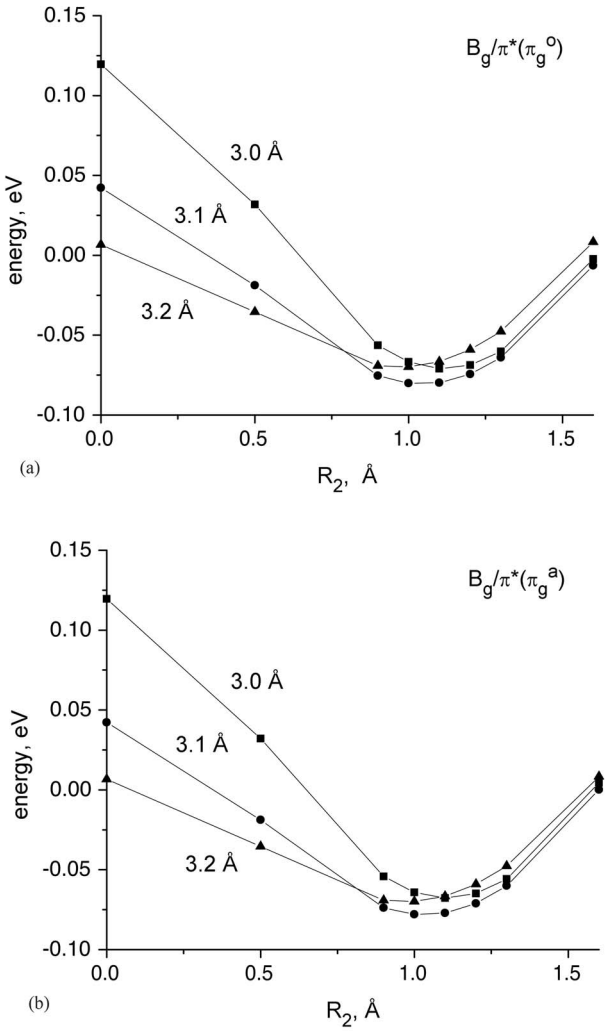

FIG. 6. PES scan along the *x* and *y* sliding coordinates at 3.0 (squares), 3.1 (rhomboids), and 3.2 Å (squares) interplanar separations.

3.6 Å. This structure of the cation is bound by 14.77 kcal/mol. The slide in the *y* direction results in a very similar binding energy of 14.86 kcal/mol. Thus at the level of theory used the *x*- and *y*-displaced structures are degener-

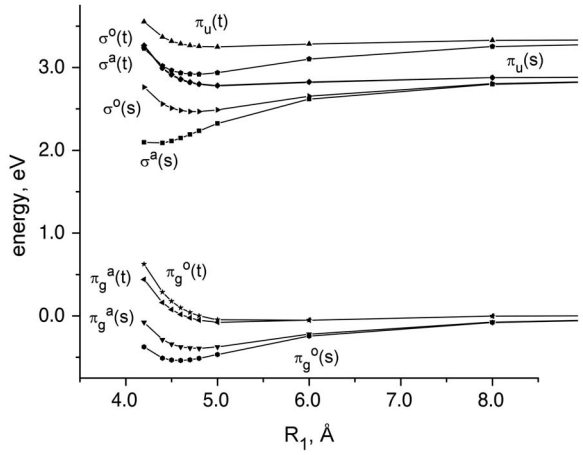

FIG. 7. Potential energy profiles along interfragment separation in t-shaped $(C_6H_6)_2^+$.

TABLE IV. IEs (eV), transition dipole moments (a.u.), and oscillator strengths of t-shaped $(C_6H_6)_2^+$.

	t-shaped			Relaxed t-shaped		
	IE	μ	f	IE	μ	f
B_2/π_g^o(stem)	8.776			8.638		
A_2/π_g^a(stem)	8.867	4.73×10^{-3}	5.0×10^{-8}	8.803	0.0135	7.40×10^{-7}
B_1/π_g^a(top)	9.163	⋯	⋯	9.193	⋯	⋯
B_2/π_g^o(top)	9.194	2.65	0.0718	9.273	2.76	0.118
A_1/σ^a(stem)	11.565	0.0928	5.88×10^{-4}	11.325	0.154	1.57×10^{-3}
B_1/σ^o(stem)	11.730	⋯	⋯	11.656	⋯	⋯
A_1/σ^a(top)	12.018	1.31×10^{-3}	1.37×10^{-7}	12.028	2.74×10^{-3}	6.25×10^{-7}
A_2/σ^o(top)	12.024	1.06×10^{-3}	8.9×10^{-8}	12.036	1.64×10^{-3}	2.23×10^{-7}
B_2/π_u(stem)	12.179	0.909	0.0688	12.110	0.829	0.0585
A_1/π_u(top)	12.490	0.278	7.03×10^{-3}	12.462	0.299	8.36×10^{-3}
E_{ref}[a]		−463.019 223			−463.016 801	

[a]Total CCSD energy (hartree) of $(C_6H_6)_2$.

ate. Two-dimensional scans shown in Fig. 6 result in a minimum energy displacement of 1.0 Å and a separation of 3.1 Å, for both the x- and y-displaced structures, the energies being 20.14 and 20.18 kcal/mol.

To summarize, our PES scans suggest that the displaced sandwich isomer is the minimum energy structure, with the BE estimated to be 20 kcal/mol, the x- and y-displaced structures being essentially degenerate.

C. Electronic states of the t-shaped isomer

We begin our discussion of the electronic states of $(C_6H_6)_2^+$ with the t-shaped isomer at its neutral equilibrium configuration. The important features of this isomer are (1) the fragments are not equivalent; (2) even when the fragments are at their neutral (D_{6h}) geometry orbital degeneracies are broken; and (3) different types of orbitals mix, i.e., π_u and σ. Excited state PES scans along the intermolecular separation coordinate are shown in Fig. 7. Vertical IEs, transition dipoles, and oscillator strengths for the electronic transitions between the cation states are listed in Table IV. The MOs and the corresponding stick spectrum are shown in Figs. 4 and 8, respectively. In the ground state, the π_g^o(stem) orbital is highest in energy and thus it is singly occupied. All the transitions discussed below involve transfer of an electron to this orbital. The corresponding vertical IE is 8.78 eV, which is 0.3 eV lower than the computed monomer value.

Orbital ordering. The MOs of the t-shaped isomer are mostly localized on individual fragments. Orbitals of the stem fragment are higher in energy than the orbitals of the top molecule. To elucidate the nature of this effect, we conducted an additional calculation in which one of the fragments is replaced by a +1 point charge at its center of mass. The structure with the stem molecule substituted by a point charge was more stable by 2.5 kcal/mol at the CCSD/6-31 $+G^*$ level. Thus it appears that the charge-multipole interactions are more favorable when the hole is localized on the stem, in agreement with predictions based on the Hunter-

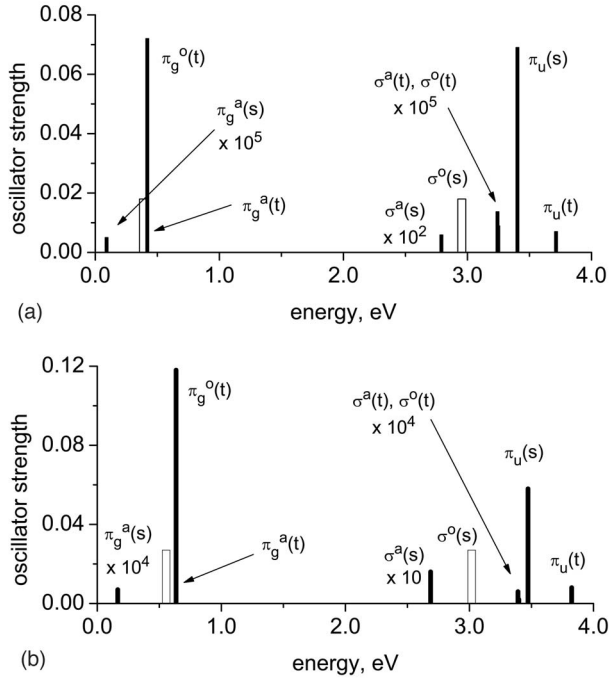

FIG. 8. Electronic states ordering and oscillator strengths of $(C_6H_6)_2^+$ at neutral (a) and relaxed (b) t-shaped configurations. Empty bars denote symmetry forbidden transitions.

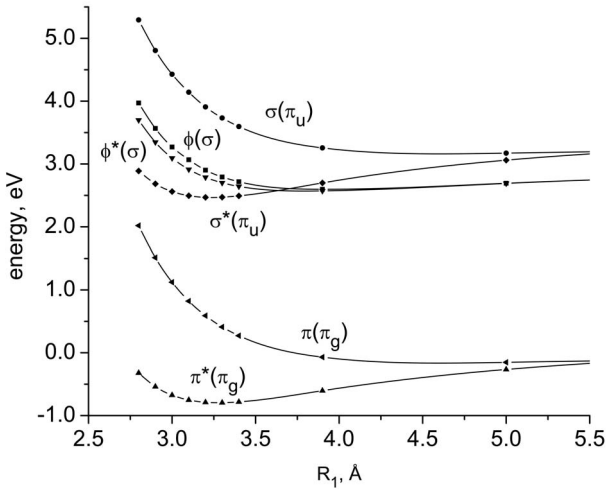

FIG. 9. Potential energy profiles along interfragment separation in sandwich $(C_6H_6)_2^+$.

TABLE V. IEs (eV), transition dipole moments (a.u.), and oscillator strengths of the sandwich and the displaced sandwich $(C_6H_6)_2^+$ isomers.

x displaced				Parallel				y displaced			
	IE	μ	f		IE	μ	f		IE	μ	f
$B_g/\pi^*(\pi_g^o)$	8.590			$E_{1g}/\pi^*(\pi_g)$	8.577			$B_g/\pi^*(\pi_g^a)$	8.592		
$A_g/\pi^*(\pi_g^a)$	8.796	⋯	⋯					$A_g/\pi^*(\pi_g^o)$	8.794	⋯	⋯
$B_u/\pi(\pi_g^a)$	8.889	0.0197	2.83×10^{-5}	$E_{1u}/\pi(\pi_g)$	9.111	3.27	0.140	$B_u/\pi(\pi_g^o)$	8.890	0.0210	3.21×10^{-6}
$A_u/\pi(\pi_g^o)$	9.137	3.23	0.140					$A_u/\pi(\pi_g^a)$	9.136	3.23	0.139
$B_g/\phi(\sigma^o)$	11.764	⋯	⋯	$E_{2u}/\phi^*(\sigma)$	11.753	3.02×10^{-3}	7.12×10^{-7}	$B_u/\phi^*(\sigma^a)$	11.761	0.133	1.37×10^{-3}
$B_u/\phi^*(\sigma^a)$	11.765	0.152	1.80×10^{-3}					$A_g/\phi(\sigma^a)$	11.766	⋯	⋯
$A_u/\phi^*(\sigma^o)$	11.766	0.101	7.98×10^{-4}	$E_{2g}/\phi(\sigma)$	11.779	⋯	⋯	$A_u/\phi^*(\sigma^o)$	11.773	0.0544	2.31×10^{-4}
$A_g/\phi(\sigma^a)$	11.778	⋯	⋯					$B_g/\phi(\sigma^o)$	11.775	⋯	⋯
$B_u/\sigma^*(\pi_u)$	11.883	0.821	0.0544	$A_{2u}/\sigma^*(\pi_u)$	11.881	0.831	0.0559	$B_u/\sigma^*(\pi_u)$	11.883	0.824	0.0547
$A_g/\sigma(\pi_u)$	12.496	⋯	⋯	$A_{1g}/\sigma(\pi_u)$	12.437	⋯	⋯	$A_g/\sigma(\pi_u)$	12.497	⋯	⋯
E_{ref}[a]		−463.018 821				−463.017 026				−463.019 035	

[a]Total CCSD energy (hartree) of $(C_6H_6)_2$.

Sanders model.[82] This model pictures an aromatic molecule as a positively charged σ framework and a negatively charged π framework. Consequently, ionizing the stem molecules allows for a favorable interaction between the positive charge and the π system of the top molecule.

PES scans. The two lowest energy states are bound and correspond to ionizations from π_g orbitals of the stem. States derived by ionizing corresponding orbitals of the top fragment are repulsive. This is in agreement with the Hunter-Sanders model, as well as the antibonding character of the corresponding DMOs. A very interesting behavior is observed for the state derived from ionization from σ^a(stem), which is actually a mixture of ionizations from the pure σ^a(stem) and π_u(top) orbitals. As the distance decreases, the weight of the latter configuration increases. Due to increased charge delocalization, this state has a higher binding energy than π_g^o(stem). In the π_u(top) state the stabilization due to delocalization is canceled out by destabilization due to placing a positive charge on the top molecules, resulting in a flat PES. The π_u(stem) state is also bound, but the orbital is more localized. The PESs of σ(top) states are rather flat, as the monomer charge distribution is not significantly altered.

Charge resonance bands. These transitions correspond to excitations within the π_g manifold of states. Due to the presence of the top molecule, the $\pi_g^a(\text{stem})\rightarrow\pi_g^o(\text{stem})$ transition becomes weakly allowed. Transitions from π_g^a(top) are symmetry forbidden. A very intense band at 0.42 eV corresponds to the $\pi_g^o(\text{top})\rightarrow\pi_g^o(\text{stem})$ excitation. Upon relaxation it shifts to 0.63 eV while its oscillator strength increases by 50%. The $\pi_g^o(\text{top})\rightarrow\pi_g^o(\text{stem})$ excitation is akin to CR bands (see Sec. III B); the initial and the final MOs are in-phase and out-of-phase combinations of the unperturbed π_g^o(top) and π_g^o(stem) monomer MOs, albeit with unequal weights. A distinguishing feature of this transition is that its dipole moment increases with decreased distance, unlike the CR bands in the sandwich isomers (see Sec. V D). This is because mixing becomes stronger at shorter distances, i.e., the decreased R_{AB} is offset by increased β (see Appendix).

Local excitations. Above 2.5 eV, transitions from the σ orbitals of the monomers appear. Excitation energies for the transitions originating from the top molecule are slightly higher. They carry little oscillator strength regardless whether the σ orbital is located on the stem or the top molecule. The $\sigma^a(\text{stem})\rightarrow\pi_g^o(\text{stem})$ is a notable exception. The acquired intensity originates from the admixtures of pure

TABLE VI. IEs (eV), transition dipole moments (a.u.), and oscillator strengths of the relaxed sandwich and the relaxed displaced sandwich $(C_6H_6)_2^+$ isomers.

x displaced				Parallel				y displaced			
	IE	μ	f		IE	μ	f		IE	μ	f
$B_g/\pi^*(\pi_g^o)$	8.105			$E_{1g}/\pi^*(\pi_g)$	8.163			$B_g/\pi^*(\pi_g^a)$	8.105		
$A_g/\pi^*(\pi_g^a)$	8.325	⋯	⋯					$A_g/\pi^*(\pi_g^o)$	8.325	⋯	⋯
$B_u/\pi(\pi_g^a)$	9.161	0.0456	5.37×10^{-5}	$E_{1u}/\pi(\pi_g)$	9.369	2.65	0.207	$B_u/\pi(\pi_g^o)$	9.161	0.0484	6.07×10^{-5}
$A_u/\pi(\pi_g^o)$	9.432	2.53	0.209					$A_u/\pi(\pi_g^a)$	9.433	2.53	0.209
$B_g/\phi(\sigma^o)$	11.707	⋯	⋯	$E_{2u}/\phi^*(\sigma)$	11.659	2.03×10^{-3}	4.07×10^{-7}	$B_u/\phi^*(\sigma^a)$	11.685	0.0744	4.86×10^{-4}
$B_u/\phi^*(\sigma^a)$	11.668	0.0741	4.79×10^{-4}					$A_g/\phi(\sigma^a)$	11.709	⋯	⋯
$A_u/\phi^*(\sigma^o)$	11.685	0.0921	7.43×10^{-4}	$E_{2g}/\phi(\sigma)$	11.751	⋯	⋯	$A_u/\phi^*(\sigma^o)$	11.668	0.0596	3.10×10^{-4}
$A_g/\phi(\sigma^a)$	11.742	⋯	⋯					$B_g/\phi(\sigma^o)$	11.739	⋯	⋯
$B_u/\sigma^*(\pi_u)$	11.367	0.795	0.0505	$A_{2u}/\sigma^*(\pi_u)$	11.429	0.801	0.0514	$B_u/\sigma^*(\pi_u)$	11.367	0.795	0.0505
$A_g/\sigma(\pi_u)$	12.792	⋯	⋯	$A_{1g}/\sigma(\pi_u)$	12.690	⋯	⋯	$A_g/\sigma(\pi_u)$	12.792	⋯	⋯
E_{ref}[a]		−463.009 538				−463.008 808				−463.009 605	

[a]CCSD energy of $(C_6H_6)_2$, in hartree.

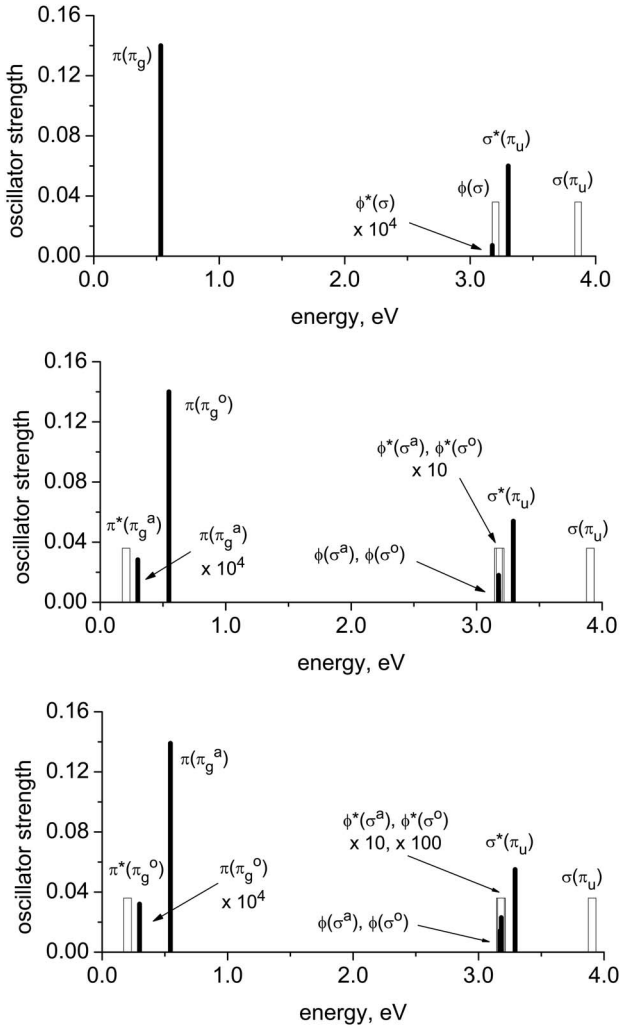

FIG. 10. Electronic states ordering and oscillator strengths of $(C_6H_6)_2^+$ at sandwich (a) and x- and y-displaced sandwich [(b) and (c)] configurations. Empty bars denote symmetry forbidden transitions.

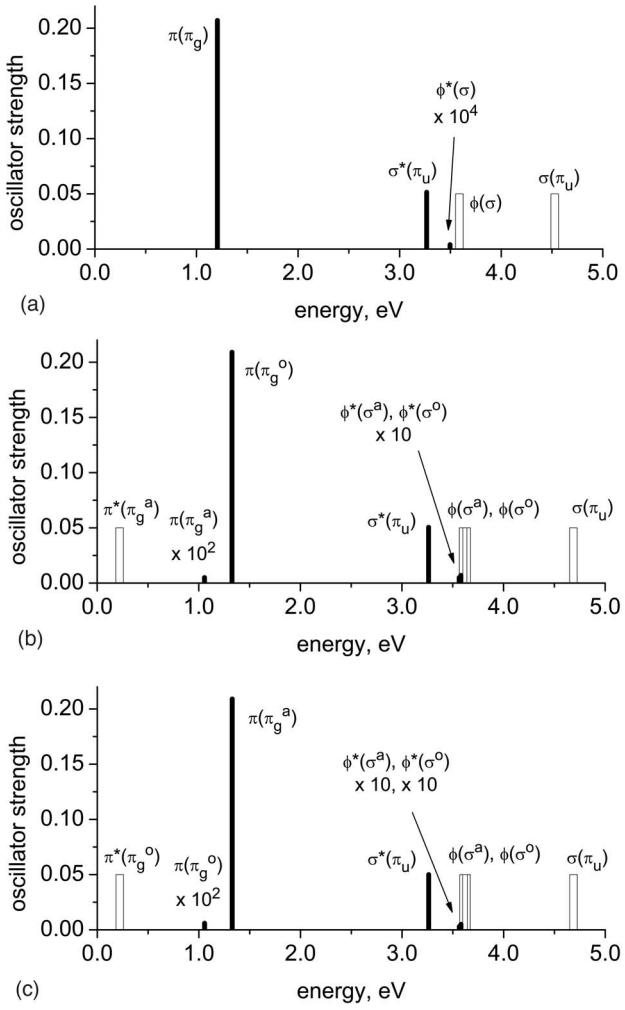

FIG. 11. Electronic states ordering and oscillator strengths of relaxed $(C_6H_6)_2^+$ at sandwich (a) and x- and y-displaced sandwich [(b) and (c)] configurations. Empty bars denote symmetry forbidden transitions.

π_u(top) and π_g^o(top) in the initial and final orbitals, respectively. The transition dipole for π_u(top) is not decreased. The decreased weight of pure π_u(top) is offset by increased weight of pure π_g^o(top). On the other hand π_u(stem) $\rightarrow \pi_g^o$(stem) loses intensity due to decreased weight of pure π_g^o(stem).

Summary. Our results for the t-shaped isomer demonstrate, quite surprisingly, that low energy strong CR bands appear even when monomers are not indistinguishable. A moderate orbital delocalization is sufficient to produce a relatively large BE, the decrease in IE, and the formation of the CR-like bands.

D. Electronic states of sandwich isomer

In the sandwich configuration, the two identical monomers form a D_{6h} structure. Excited state PES scans along the ring separation coordinate are shown in Fig. 9. Neutral and relaxed configuration energies along with transition properties are listed in Tables V and VI, respectively. The corresponding stick spectra are shown in Figs. 10(a) and 11(a). The HOMO (see Fig. 3) is the doubly degenerate $\pi^*(\pi_g)$ pair, and the corresponding vertical IE is lowered to 8.58 eV from 9.10 eV (computed) in the monomer. In the cation, this pair of orbitals hosts three electrons and the nine lowest excited states of the cation are derived from promoting an electron to this pair.

PES scans. As expected from DMO-LCFMO considerations, energies of the states derived from ionization from bonding orbitals result in repulsive PESs, while the states derived from ionizations from antibonding orbitals result in bound states. The equilibrium distances of these bound states are shorter than those of the neutral, to maximize the overlap between the FMOs. For example, the lowest $\pi^*(\pi_g)$ state is bound, whereas $\pi(\pi_g)$ is repulsive. The $\pi^*(\pi_u)$ and $\pi(\pi_u)$ states follow the same trend, while the states derived from $\phi^*(\sigma)$ and $\phi(\sigma)$ feature flat PESs, due to small overlap between the inner σ FMOs. Thus these are perhaps more correctly described as nonbonding states. The increased attraction in the $\sigma^*(\pi_u)$ state brings it below the ϕ states, which reverses the ordering of the LE bands relative to the monomer.

Charge resonance bands. The π_g orbitals of benzenes are the dimer counterparts of λ from Fig. 2 (see Sec. III A), and they are antisymmetric with respect to inversion in the dimer frame. Strong CR bands corresponding to transitions

between bonding and complementary antibonding combinations of π_g are expected to dominate the spectrum. At the neutral dimer geometry, the band occurs at 0.53 eV and has a transition dipole of 3.27 a.u. This value is very close to half the distance between monomers, 3.68 a.u, as follows from Eq. (10). As one can see from PES scans, the excitation energy of the CR band increases upon relaxation and reaches 1.21 eV around the minimum. Although the transition dipole moment decreases due to shorter interfragment distance following Eq. (10), the band gains oscillator strength due to the increase in excitation energy.

Local excitations. The σ and π_u orbitals are counterparts of the ν orbitals of Sec. III A and they are symmetric with respect to inversion. Thus, the dipole allowed electronic transitions are of the case II type (Fig. 2), that is, transitions from the antibonding combinations of σ and π_u to the antibonding combination of π_g. As follows from the analysis Sec. III A, the intensities of these bands should be similar to the corresponding monomer transitions, i.e., the transition from σ will be weak (dipole forbidden but vibronically allowed $\tilde{B}$ band), while the transition from π_u will be relatively strong ($\tilde{C}$ band of the monomer). LE bands occur above 3 eV. As predicted, transitions from $\phi^*(\sigma)$ and $\phi(\sigma)$ are weak and symmetry forbidden, respectively. The intensity presumably arises from the relatively small interfragment terms in Eqs. (6) and (8). The allowed transition from $\sigma^*(\pi_u)$ is at 3.30 eV at neutral configuration. Its dipole moment is slightly lower than in the monomer due to intermolecular terms appearing in Eqs. (6) and (8). Its position changes insignificantly upon relaxation.

The symmetry forbidden $\sigma(\pi_u) \rightarrow \pi^*(\pi_g)$ excitation is at 3.86 eV. Decreased interfragment distance in the dimer cation causes it to shift 4.53 eV. A very important feature is the (explained above) reversed order of the allowed and the forbidden bands in the 3.0–3.5 eV region: the strong $\sigma^*(\pi_u)$ transition is now at a lower energy than the ϕ band, which shifted from 3.2 to 3.5 eV.

Summary. The sandwich isomer illustrates the application of the DMO-LCFO framework developed in Sec. III A. The spectrum is clearly separated into the charge resonance and local excitation parts. Geometric relaxation from the neutral to the cation produces pronounced changes in the spectrum: the CR band shifts to the blue and gains intensity, while LE bands reverse their order.

E. Electronic states of displaced sandwich isomers

Displaced sandwich structures are derived from the sandwich by sliding the monomers relative to each other in either x or y direction. Figure 12 presents PES scans in x and y directions starting from the D_{6h} sandwich structure. The behavior of the states in both cases is complementary and similar to JT distortions: states that are stabilized by the displacement in one direction are destabilized by the displacement in the other. The only exception are the states derived from the monomer π_u orbitals due to their cylindrical symmetry. A similar behavior was observed in the monomer relaxation to acute and obtuse geometries.

IEs, transition dipoles, and oscillator strengths for transitions between cation states are given in Table V and Figs.

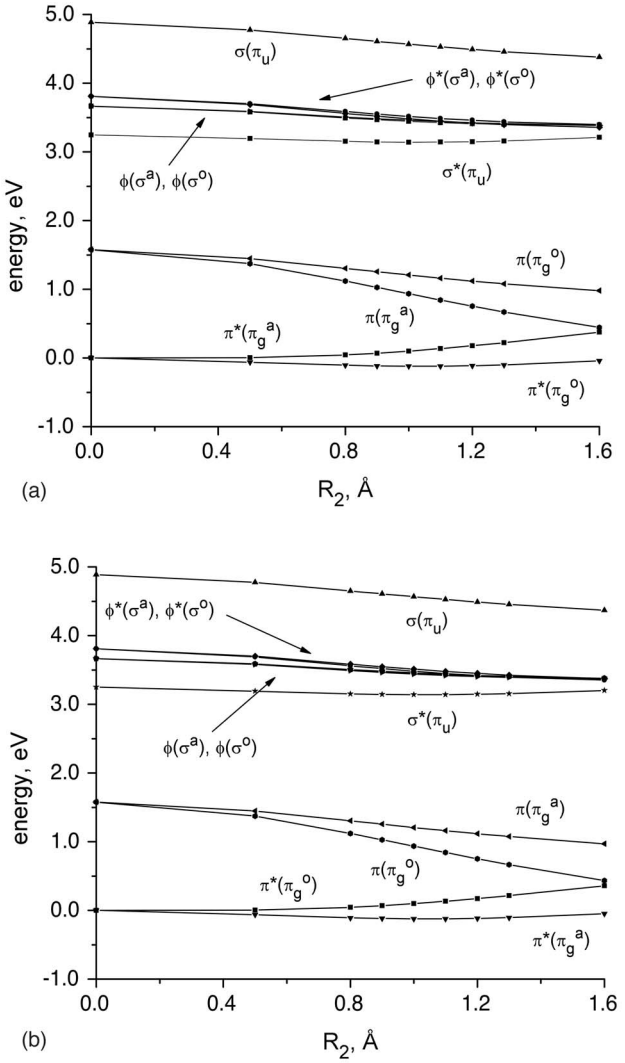

FIG. 12. Potential energy profiles along interfragment sliding in (a) x- and (b) y-displaced sandwich $(C_6H_6)_2^+$. Interplanar separation was held fixed at 3.1 Å.

10(b) and 10(c). Overall, these are remarkably similar to the sandwich isomer. The displacement results in only minor differences in IE between the x and y isomers, i.e., the first IE 8.59 in both cases.

PES scans. Due to the lower symmetry, the degeneracy between $\pi^*(\pi_g^o)$ and $\pi^*(\pi_g^a)$ is lifted, as is the degeneracy between the $\pi(\pi_g)$ pair. Overall, the PES is rather flat in the ground state. The energy dependence is more sharp for $\pi^*(\pi_g^a)$ and $\pi(\pi_g^a)$ for x sliding coordinate, and $\pi^*(\pi_g^o)$ and $\pi(\pi_g^o)$ for sliding in the y direction. In the 3 eV energy region, no reordering of states due to displacement occurs. The components of $\phi^*(\sigma)$ and $\phi(\sigma)$ are no longer degenerate; however, the splitting is small.

Charge resonance bands. In the x-displaced isomer the highest, singly occupied orbital is $\pi^*(\pi_g^o)$. The complementary $\pi(\pi_g^o)$ orbital is 0.55 eV lower. As in the sandwich, this transition is very intense, due to the nature of initial and final orbitals. Upon relaxation the band shifts to 1.33 eV. In between these two orbitals, there are the $\pi^*(\pi_g^a)$ and $\pi(\pi_g^a)$ FMOs. The transition to the latter is now symmetry allowed but carries little oscillator strength. In the y-displaced isomer,

the roles of constituent π_g^o and π_g^a are simply reversed. The energy gaps between the levels remain nearly the same.

Local excitations. Higher in energy, at approximately 3.2 eV, we find the ϕ states within 0.1 eV from each other. Although dipole allowed in the displaced structures, these transitions carry essentially no oscillator strength. The excitation to $\sigma^*(\pi_u)$ at 3.3 eV is symmetry allowed and is fairly intense, just like in the monomer. The $\sigma(\pi_u)$ state is 0.6 eV higher, but it is symmetry forbidden. Upon relaxation to the cation structure the ordering of bands changes, as already discussed in Sec. V D.

Summary. Overall, the displacement plays a relatively minor role in changing the electronic spectrum of the sandwich-type isomers. Its major effect is breaking the orbital and state degeneracies, which leads to the two structures with different orbital characters and state ordering but nearly identical spectral signatures. Symmetry reduction and breaking the degeneracies result in additional lines, most importantly, below the major CR band.

VI. DISCUSSION

Ionization of the benzene dimer drastically changes its bonding character from van der Waals to covalent. The change is particularly significant in the sandwich-type isomers, where the HOMO has strong antibonding character with respect to the two fragments. Even in the singly occupied HOMO of the t-shaped structure, where fragments are no longer equivalent and orbitals are more localized, the fragment orbitals interfere destructively in the region between monomers, i.e., have antibonding character. In the neutral species, the t-shaped and displaced sandwich isomers are nearly degenerate; the calculated energy difference is less than 0.1 kcal/mol. Ionization of the dimer stabilizes most strongly the displaced sandwich isomer, and its binding energy increases to 20 kcal/mol, whereas the binding energy of the t-shaped isomer becomes 12 kcal/mol. Thus, it seems unlikely that the t-shaped isomer will be produced in the experiments of Refs. 33 and 34. This supports the conclusions of the hole-burning study, which indicated the presence of a single isomer in the molecular beam.[34] A t-shaped isomer will, however, be initially formed in femtosecond ionization experiments and subsequently isomerize to a displaced sandwich. This evolution can in principle be resolved.

Using a diabatic state framework, we can also comment on the nature of binding in the dimer cations. In the sandwich, the BEs are 0.51 and 0.67 eV at the neutral and relaxed configurations, respectively. The diabatic states, which correspond to the charge being localized on one of the fragments, see Eq. (11), are exactly degenerate at the sandwich geometry because both monomers are the same, and thus the coupling between these states is half the splitting between $\pi^*(\pi_g)$ and $\pi(\pi_g)$. At the neutral and relaxed geometries, the couplings are 0.27 and 0.60 eV, respectively (the interfragment distance changes from 3.9 to 3.3 Å). The remaining 0.24 and 0.07 eV of interaction is the interaction between the hole and a neutral benzene, i.e., the binding energy of the diabatic state. Diabatic BE actually decreases in the dimer cation relative to the neutral geometry and the total binding is almost exclusively due to charge transfer forces. The binding energies of the t-shaped isomer are 0.39 and 0.46 eV at the neutral and relaxed configurations, respectively. Using the generalized Mulliken-Hush model,[71] we calculated the couplings to be 0.21 and 0.23 eV, while the binding energies of the diabatic state with the hole localized on the stem molecule are 0.19 and 0.36 eV. Thus, due to the larger distance the electrostatic interactions play a more significant role in the t-shaped than in the sandwich isomer.

An interesting question is about the mechanism of stabilization of the displaced sandwich structure relative to the sandwich. In the neutral species, electrostatic interactions, as described in the Hunter-Sanders model, are the driving force, whereas in the cation, the displacement plays a role of a JT mode lifting degeneracy between the two states. Both effects are characterized by similar energies. In the neutral, the displacement in the sandwich is associated with a 1 kcal/mol gain in binding energy, while the cation value is not much higher, 2 kcal/mol. The monomer relaxation leads to 4 kcal/mol of additional stabilization. Thus, it is not clear whether the displacement is driven by Hunter-Sanders electrostatic interactions, JT effect, or if the two contribute equally. Full geometry optimization will address the relative importance of the two effects. Further frequency calculations would allow us to characterize the displaced structures as two minima, or, perhaps, a minimum and a transition state.

The photodissociation action spectra of the dimer cation exhibit peaks at 1.07, 1.35, 2.14, and 2.82 eV.[33] The two relaxed displaced structures exhibit essentially identical spectra, with excited electronic states at 1.06, 1.33, 3.26, and 3.57 eV. The positions of the two low energy CR bands agree extremely well with the experiment; however, their intensity pattern does not. Experimentally, the ratio is 1:10, whereas the calculated ratio is 1:1000. The discrepancy could be due to strong vibronic interactions between the two states.

With the current level of theory, the excitation energies of the $\pi_u \rightarrow \pi_g$ and $\sigma \rightarrow \pi_g$ transitions of the monomer ($\tilde{B}$ and $\tilde{C}$ bands) are overestimated by 0.5 and 0.6 eV, respectively. If this correction is applied to the dimer, it yields 2.76 and 2.97 eV for the LE bands. The lower energy transition, which corresponds to $\pi_u \rightarrow \pi_g$, agrees rather poorly with the experimental peak at 2.14 eV; however, the agreement for $\sigma \rightarrow \pi_g$ (2.82 vs 2.97 eV) is much better. Most importantly, our study demonstrated that the two bands reverse their order relative to the monomer. Again, the intensity pattern is not reproduced, because the dipole-forbidden $\tilde{B}$ band of the monomer borrows intensity due to vibronic interactions.[83] Additionally, the ϕ excited states have nonbonding character, while the σ states are bound. This may affect the observed intensity pattern in the photodissociation action spectrum. The large errors in the predicted excitation energies for LE transitions are typical of the EOM-IP-CCSD method.[84,85] They arise due to inclusion of only singly excited determinants (with respect to the ionized state) in the wave function. Note that the complementary nature of states involved in the CR transitions results in error cancellation and significantly more accurate transition energies.

Previous studies often discounted the t-shaped dimer cation structure as a source of the CR bands because of the overlap considerations. Our calculations demonstrate, however, that such bands are also present in the t-shaped isomer and have considerable intensity due to partial delocalization of the FMOs. The oscillator strength is approximately half of that of the sandwiches. It would be interesting to investigate the effect of monomer relaxation on the intensity of the bands. Two scenarios are possible. The hole may localize on the stem molecule, which would further localize orbitals and, therefore, reduce the intensity. Alternatively, the JT distortion may bring the stem and top orbitals closer together thus allowing for more delocalization, which will yield stronger CR bands.

The knowledge of both t-shaped and sandwich isomer spectra is useful from the point of view of studying ionization chemistry of aromatic solvents using femtosecond techniques. Neutron diffraction experiments on liquid benzene point to perpendicular orientation of nearest neighbors;[86] thus the t-shaped isomer will be initially produced. Subsequent nuclear dynamics will lead to charge delocalization and formation of sandwich dimer cations. This process could be probed by monitoring the position and intensity of the CR band. Initially it would appear near 0.42 eV (2950 nm), as calculated for the neutral t-shaped geometry. The monomer cation would then evolve towards the displaced sandwich dimer cation, with the two rings rotating and coming closer together. During this process the intensity of the CR band would double and shift to 1.33 eV (940 nm). Such a pronounced change in the spectrum should be easily resolved.

VII. CONCLUSIONS

This paper reports a thorough study of the electronic states of the benzene dimer cation. Energies of the ten lowest electronic states of the dimer, as well as oscillator strengths for electronic transitions, are calculated by EOM-IP-CCSD/6-31+G*. Several isomers and relaxation coordinates are considered. The hallmark of the calculated spectra are the charge resonance bands, which appear both in the t-shaped and sandwich isomers. Their position and intensity can serve as extremely sensitive probe of the dimer structure. For example, the CR bands allow us to assign the displaced sandwich isomer as the ground state of the $(C_6H_6)_2^+$ system. Moreover, our results offer support to studies aiming to resolve the dynamics of cation formation using femtosecond spectroscopy. Lastly, inversion of LE bands has been observed in the lowest energy displaced sandwich structure. This may hint at different relaxation dynamics in the cation monomer and dimer. The trends in electronic spectrum are explained by a simple DMO-LCFMO model. The results explain the nature of the intense CR bands and less intense LE transitions of the dimer and outline the evolution of the dimer electronic spectrum upon ionization.

ACKNOWLEDGMENTS

This work was conducted in the framework of the Center for Computational Studies of Electronic Structure and Spectroscopy of Open-Shell and Electronically Excited Species supported by the National Science Foundation through the CRIF:CRF CHE-0625419+0624602+0625237 grant. Two of the authors (A.I.K. and S.E.B.) also gratefully acknowledge support of the National Science Foundation through the CHE-0616271 and CHE-0617060 grants, respectively. They wish to thank the University of Southern California Center for High Performance Computing and Communications for making their computational resources available and technical support throughout this project. One of the authors (A.I.K.) would like to thank Professor Masaaki Fujii and Dr. Miyazaki Mitsuhiko from Yokohama Institute of Technology for their insightful comments, exciting discussions, and sharing the results of their work prior to publication. They also acknowledge collaboration with Professor C. David Sherrill from Georgia Tech.

APPENDIX: DMO-LCFMO TREATMENT OF NONEQUIVALENT ARGUMENTS

Here we apply the DMO-LCFMO framework for the case of nonequivalent fragments, which is similar to heteronuclear diatomics, where MOs are no longer equal mixtures of AOs and symmetry-imposed selection rules do not apply. When monomers become nonequivalent, the relative weights of the fragment orbitals in the dimer MOs change and the terms in Eq. (4) do not cancel out; thus, both the $\psi_+(\lambda) \rightarrow \psi_-(\lambda)$ and the $\psi_+(\lambda) \rightarrow \psi_-(\lambda)$ transitions become allowed. The resulting DMOs are

$$\psi_-(\lambda) = \frac{1}{\sqrt{(1+\beta^2-2\beta s_{\lambda\lambda})}}(\beta\lambda_A - \lambda_B), \tag{A1}$$

$$\psi_+(\lambda) = \frac{1}{\sqrt{(1+\beta^2+2\beta s_{\lambda\lambda})}}(\lambda_A + \beta\lambda_B), \tag{A2}$$

$$\psi_-(\nu) = \frac{1}{\sqrt{(1+\beta^2-2\beta s_{\nu\nu})}}(\beta\nu_A - \nu_B), \tag{A3}$$

$$\psi_+(\nu) = \frac{1}{\sqrt{(1+\beta^2+2\beta s_{\nu\nu})}}(\nu_A + \beta\nu_B), \tag{A4}$$

where $0 \leqslant \beta \leqslant 1$. The case of equivalent fragments is recovered when $\beta = 1$. The transition dipole moments are

$$\langle\psi_+(\nu)|\mu|\psi_-(\lambda)\rangle = \frac{1}{\sqrt{(1+\beta^2+2\beta s_{\nu\nu})(1+\beta^2-2\beta s_{\lambda\lambda})}} \times (2\beta\langle\nu_A|\mu|\lambda_A\rangle + (1+\beta^2)\langle\nu_B|\mu|\lambda_A\rangle), \tag{A5}$$

$$\langle\psi_+(\nu)|\mu|\psi_+(\lambda)\rangle = \frac{1-\beta^2}{\sqrt{(1+\beta^2+2\beta s_{\nu\nu})(1+\beta^2+2\beta s_{\lambda\lambda})}} \times (\langle\nu_A|\mu|\lambda_A\rangle), \tag{A6}$$

where we assumed that the symmetry rules for case I transi-

tions still apply. Thus, a weaker line will appear at lower energy. Likewise, for the case II transitions, a higher energy transition will become allowed. Consider now the transition within the ν manifold:

$$\langle \psi_+(\nu)|\mu|\psi_-(\nu)\rangle = \frac{1}{\sqrt{(1+\beta^2+2\beta s_{\nu\nu})(1+\beta^2-2\beta s_{\nu\nu})}} \times (\beta\langle \nu_A|\mu|\nu_A\rangle - \beta\langle \nu_B|\mu|\nu_B\rangle - \langle \nu_A|\mu|\nu_B\rangle + \beta^2\langle \nu_B|\mu|\nu_A\rangle) \quad \text{(A7)}$$

$$= \frac{\beta R_{AB}}{\sqrt{(1+\beta^2+2\beta s_{\nu\nu})(1+\beta^2-2\beta s_{\nu\nu})}}. \quad \text{(A8)}$$

This is an analog of the CR transition, with the intensity decreased by a factor of β compared to the symmetric case.

[1] W. Saenger, *Principles of Nucleic Acid Structure* (Springer-Verlag, New York, 1984).
[2] S. K. Burley and G. A. Petsko, Science **229**, 23 (1985).
[3] C. A. Hunter, J. Singh, and J. M. Thornton, J. Mol. Biol. **218**, 837 (1991).
[4] P. Hobza, R. Zahradnik, and K. Müller-Dethlefs, Collect. Czech. Chem. Commun. **71**, 443 (2006).
[5] K. Müller-Dethlefs and P. Hobza, Chem. Rev. (Washington, D.C.) **100**, 143 (2000).
[6] B. Askew, P. Ballester, C. Buhr, K. S. Jeong, S. Jones, K. Parris, K. Williams, and J. Rebek, Jr., J. Am. Chem. Soc. **111**, 1082 (1989).
[7] C. A. Hunter, Chem. Soc. Rev. **23**, 101 (1994).
[8] J. Rebek, Jr., Chem. Soc. Rev. **25**, 255 (1996).
[9] E. A. Meyer, R. K. Castellano, and F. Diederich, Angew. Chem., Int. Ed. **42**, 1210 (2003).
[10] C. G. Claessens and J. F. Stoddart, J. Phys. Org. Chem. **10**, 254 (1997).
[11] A. Sancar, Biochemistry **33**, 2 (1994).
[12] M. Bixon and J. Jortner, J. Phys. Chem. A **105**, 10322 (2001).
[13] F. L. Gervasio, A. Laio, M. Parrinello, and M. Boero, Phys. Rev. Lett. **94**, 158103 (2005).
[14] V. J. Chebny, R. Shukla, and R. Rathore, J. Phys. Chem. A **110**, 13003 (2006).
[15] E. R. Bittner, J. Chem. Phys. **125**, 094909 (2006).
[16] Y. Inokuchi, Y. Naitoh, K. Ohashi, K. Saitow, K. Yoshihara, and N. Nishi, Chem. Phys. Lett. **269**, 298 (1997).
[17] K. Okamoto, A. Saeki, T. Kozawa, Y. Yoshida, and S. Tagawa, Chem. Lett. **32**, 834 (2003).
[18] K. Enomoto, J. A. LaVerne, and M. S. Araos, J. Phys. Chem. A **111**, 9 (2007).
[19] W. Cencek, M. Jeziorska, R. Bukowski, M. Jaszunski, B. Jeziorski, and K. Szalewicz, J. Phys. Chem. A **108**, 3211 (2004).
[20] K. P. Huber and G. Herzberg, *Constants of Diatomic Molecules* (Van Nostrand Reinhold, New York, 1979).
[21] M. C. Castex, J. Chem. Phys. **74**, 759 (1981).
[22] L. Flamigni, N. Camaioni, P. Bortolus, F. Minto, and M. Gleria, J. Phys. Chem. **95**, 971 (1991).
[23] A. L. L. East and E. C. Lim, J. Chem. Phys. **113**, 8981 (2000).
[24] B. Minaev, Phys. Chem. Chem. Phys. **5**, 2314 (2003).
[25] L. Mohanambe and S. Vasudevan, J. Phys. Chem. B **110**, 14345 (2006).
[26] R. Lindner, K. Müller-Dethlefs, E. Wedum, K. Haber, and E. R. Grant, Science **271**, 1698 (1996).
[27] K. Müller-Dethlefs and J. Barrie Peel, J. Chem. Phys. **111**, 10550 (1999).
[28] M. Ford, R. Lindner, and K. Müller-Dethlefs, Mol. Phys. **101**, 705 (2003).
[29] W. Radloff, V. Stert, T. Freudenberg, I. V. Hertel, C. Jouvet, C. Dedonder-Lardeux, and D. Solgadi, Chem. Phys. Lett. **281**, 20 (1997).
[30] T. Hirata, H. Ikeda, and H. Saigusa, J. Phys. Chem. A **103**, 1014 (1999).
[31] K. Ohashi and N. Nishi, J. Chem. Phys. **95**, 4002 (1991).
[32] K. Ohashi and N. Nishi, J. Phys. Chem. **96**, 2931 (1992).
[33] K. Ohashi, Y. Nakai, T. Shibata, and N. Nishi, Laser Chem. **14**, 3 (1994).
[34] K. Ohashi, Y. Inokuchi, and N. Nishi, Chem. Phys. Lett. **263**, 167 (1996).
[35] T. Shida and W. H. Hamill, J. Chem. Phys. **44**, 4372 (1966).
[36] B. Badger and B. Brockleh, Trans. Faraday Soc. **65**, 2582 (1969).
[37] J. R. Grover, E. A. Walters, and E. T. Hui, J. Phys. Chem. **91**, 3233 (1987).
[38] H. Krause, B. Ernstberger, and H. J. Neusser, Chem. Phys. Lett. **184**, 411 (1991).
[39] F. H. Field, P. Hamlet, and W. F. Libby, J. Am. Chem. Soc. **91**, 2939 (1969).
[40] M. Meot-Ner (Mautner), P. Hamlet, E. P. Hunter, and F. H. Field, J. Am. Chem. Soc. **100**, 5466 (1978).
[41] K. Hiraoka, S. Fujimaki, K. Aruga, and S. Yamabe, J. Chem. Phys. **95**, 8413 (1991).
[42] M. Rusyniak, Y. Ibrahim, E. Alsharaeh, M. Meot-Ner (Mautner), and M. S. El-Shall, J. Phys. Chem. A **107**, 7656 (2003).
[43] Y. Ibrahim, E. Alsharaeh, M. Rusyniak, S. Watson, M. Meot-Ner (Mautner), and M. S. El-Shall, Chem. Phys. Lett. **380**, 21 (2003).
[44] S. A. Milosevich, K. Saichek, L. Hinchey, W. B. England, and P. Kovacic, J. Am. Chem. Soc. **105**, 1088 (1983).
[45] E. Miyoshi, T. Ichikawa, T. Sumi, Y. Sakai, and N. Shida, Chem. Phys. Lett. **275**, 404 (1997).
[46] E. Miyoshi, N. Yamamoto, M. Sekiya, and K. Tanaka, Mol. Phys. **101**, 227 (2003).
[47] Y. Itagaki, N. P. Benetis, R. M. Kadam, and A. Lund, Phys. Chem. Chem. Phys. **2**, 2683 (2000).
[48] J. B. Birks, *Photophysics of Aromatic Molecules* (Wiley, New York, 1970).
[49] See EPAPS Document No. E-JCPSA6-127-304725 for the equilibrium geometries of the benzene and benzene dimer cations and PES scans along important relaxation coordinates. This document can be reached through a direct link in the online articles' HTML reference section or via the EPAPS homepage (http://www.aip.org/pubservs/epaps.html/).
[50] J. M. Steed, T. A. Dixon, and W. Klemperer, J. Chem. Phys. **70**, 4940 (1979).
[51] E. Arunan and H. S. Gutowsky, J. Chem. Phys. **98**, 4294 (1993).
[52] P. Hobza, H. L. Selzle, and E. W. Schlag, J. Phys. Chem. **100**, 18790 (1996).
[53] S. Sun and E. R. Bernstein, J. Phys. Chem. **100**, 13348 (1996).
[54] R. L. Jaffe and G. D. Smith, J. Chem. Phys. **105**, 2780 (1996).
[55] M. O. Sinnokrot and C. D. Sherrill, J. Phys. Chem. A **108**, 10200 (2004).
[56] M. O. Sinnokrot and C. D. Sherrill, J. Phys. Chem. A **110**, 10656 (2006).
[57] R. Podeszwa, R. Bukowski, and K. Szalewicz, J. Phys. Chem. A **110**, 10345 (2006).
[58] M. E. Akopian, F. I. Vilesov, and A. N. Terenin, Sov. Phys. Dokl. **6**, 490 (1961).
[59] P. Baltzer, L. Karlsson, B. Wannberg, G. Ohrwall, D. M. P. Holland, M. A. MacDonald, M. A. Hayes, and W. von Niessen, Chem. Phys. **224**, 95 (1997).
[60] E. E. Rennie, C. A. F. Johnson, J. E. Parker, D. M. P. Holland, D. A. Shaw, and M. A. Hayes, Chem. Phys. **229**, 107 (1998).
[61] A. J. Yencha, R. I. Hall, L. Avaldi, G. Dawber, A. G. McConkey, M. A. MacDonald, and G. C. King, Can. J. Chem. **82**, 1061 (2004).
[62] H.-G. Weikert and L. S. Cederbaum, Chem. Phys. Lett. **237**, 1 (1997).
[63] K. Takeshita, Theor. Chem. Acc. **103**, 64 (1999).
[64] M. Doscher, H. Koppel, and P. G. Szalay, J. Chem. Phys. **117**, 2645 (2002).
[65] H. Koppel, M. Doscher, I. Baldea, H. D. Meyer, and P. G. Szalay, J. Chem. Phys. **117**, 2657 (2002).
[66] R. A. Marcus, Discuss. Faraday Soc. **29**, 21 (1960).
[67] R. A. Marcus, J. Chem. Phys. **43**, 679 (1965).
[68] R. A. Marcus and N. Sutin, Biochim. Biophys. Acta **811**, 265 (1985).
[69] P. W. Atkins and R. S. Friedman, *Molecular Quantum Mechanics* (Oxford University Press, New York, 2005).
[70] R. S. Mulliken and W. B. Person, *Molecular Complexes* (Wiley-Interscience, New York, 1969).
[71] R. J. Cave and M. D. Newton, Chem. Phys. Lett. **249**, 15 (1996).
[72] D. Sinha, D. Mukhopadhyay, and D. Mukherjee, Chem. Phys. Lett. **129**, 369 (1986).
[73] D. Sinha, D. Mukhopadhya, R. Chaudhuri, and D. Mukherjee, Chem. Phys. Lett. **154**, 544 (1989).
[74] R. Chaudhuri, D. Mukhopadhyay, and D. Mukherjee, Chem. Phys. Lett. **162**, 393 (1989).
[75] J. F. Stanton and J. Gauss, J. Chem. Phys. **111**, 8785 (1999).
[76] P. A. Pieniazek, S. A. Arnstein, S. E. Bradforth, A. I. Krylov, and C. D. Sherrill (unpublished).
[77] G. D. Purvis and R. J. Bartlett, J. Chem. Phys. **76**, 1910 (1982).

[78] H. Sekino and R. J. Bartlett, Int. J. Quantum Chem., Quantum Chem. Symp. **18**, 255 (1984).
[79] J. F. Stanton and R. J. Bartlett, J. Chem. Phys. **98**, 7029 (1993).
[80] Y. Shao, L. Fusti-Molnar, Y. Jung, *et al.* Phys. Chem. Chem. Phys. **8**, 3172 (2006).
[81] J. Gauss and J. F. Stanton, J. Phys. Chem. A **104**, 2865 (2000).
[82] C. A. Hunter and J. K. M. Sanders, J. Am. Chem. Soc. **112**, 5525 (1990).
[83] H. Köppel and L. S. Cederbaum, J. Chem. Phys. **89**, 2023 (1988).
[84] S. Hirata, M. Nooijen, and R. J. Bartlett, Chem. Phys. Lett. **328**, 459 (2000).
[85] M. Kamiya and S. Hirata, J. Chem. Phys. **125**, 074111 (2006).
[86] M. Misawa and T. Fukunaga, J. Chem. Phys. **93**, 3496 (1990).